Inorganic Chemistry

ARTICLE

pubs.acs.org/IC

Effects of the Central Lanthanide Ion Crystal Radius on the 15-MC$_{Cu^{II}(N)pheHA}$-5 Structure

Curtis M. Zaleski,[§] Choong-Sun Lim,[†] Annabel D. Cutland-Van Noord,[†] Jeff W. Kampf,[†] and Vincent L. Pecoraro*[,†]

[†]Department of Chemistry, University of Michigan, Ann Arbor, Michigan 48108-1005, United States

[§]Department of Chemistry, Shippensburg University, Shippensburg, Pennsylvania 17257-2200, United States

Supporting Information

ABSTRACT: Twenty crystal structures of the $Ln^{III}[15\text{-}MC_{CuII(N)pheHA}\text{-}5]^{3+}$ complex, where pheHA = phenylalanine hydroxamic acid and where $Ln^{III} = Y^{III}$ and $La^{III}-Tm^{III}$, except Pm^{III}, with the nitrate and/or hydroxide anion are used to assess the effect of the central metal ion on the metallacrown structure. Each $Ln^{III}[15\text{-}MC_{CuII(N)pheHA}\text{-}5]^{3+}$ complex is amphiphilic with a hydrophobic side consisting of the phenyl groups of the pheHA ligand and a side without the aromatic residues. Three general structures are observed for the $Ln^{III}[15\text{-}MC_{CuII(N)pheHA}\text{-}5]^{3+}$ complexes. In the Type 1 structures, the central metal ion does not bind a nitrate anion on the metallacrown's hydrophobic face, and two adjacent metallacrowns dimerize through their phenyl groups producing a hydrophobic compartment. In the Type 2 structures, the central metal ion binds a nitrate in a bidentate fashion on the hydrophobic face. There are two distinct types of Type 2 metallacrowns, designated A and B. Type 2A metallacrowns have a water molecule bound to the central metal ion on the hydrophilic face, while Type 2B metallacrowns have a monodentate nitrate ion bound on the hydrophilic face to the central metal ion. The Type 2 metallacrowns also dimerize via the phenyl groups to form a hydrophobic compartment. In Type 3 structures, the central metal ion binds a nitrate in a bidentate fashion on the hydrophobic side, but instead of forming dimers, the metallacrowns pack in a helical arrangement to give either *P* or *M* one-dimensional helices. Regardless of the type of metallacrown, the overall trend observed is that as the Ln^{III} ion crystal radius increases, the metallacrown cavity radius also increases while the metallacrown becomes more planar. This conclusion is demonstrated by a decrease in the oxime oxygen distances to the oxime oxygen mean plane and a decrease in the ring Cu^{II} distances to the Cu^{II} mean plane as the metallacrown cavity radius increases and the lanthanide crystal radius increases. In addition, a decrease in the $O_{oxime}-Cu^{II}-N_{oxime}-O_{oxime}$ torsion (dihedral) angles is also observed as the metallacrown cavity radius and the lanthanide crystal radius both increase. These observations help explain the thermodynamic preferences for Ln^{III} ions within this class of metallacrowns and may be used to design compartments capable of binding guests in different orientations within chiral, soft solids.

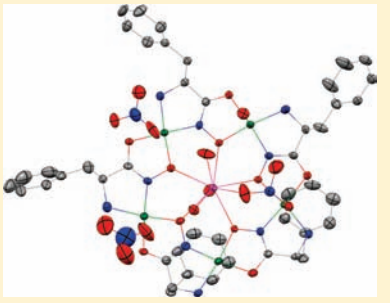

INTRODUCTION

Planar 15-MC-5 complexes are one member of the growing family of molecules known as metallacrowns (MC).[1] The complexes are extremely versatile with structures ranging from 9-MC-3[2] to 60-MC-20.[3] They have been prepared with numerous metals and organic ligands, adopt a variety of molecular architectures, and can form homochiral solids,[4] microporous arrays[4] and chiral compartments for guest sequestration.[5] Potential applications include use as MRI contrasting agents,[6] separations or nonlinear optical technology using homochiral solids,[7,8] sensor applications exploiting selective anion binding[9] and molecular magnets.[10] While 3-dimensional shaped 15-MC-5 had been reported with salicylhydroxamic acid and manganese,[11] the first planar 15-MC-5 complexes were made with Cu^{II} and the ligand picoline hydroxamic acid, which places the ring metal ions at 108° with respect to each other.[12] A similar topology can be achieved with α-amino hydroxamic acids.[13] The use of α-amino acid derivatives as ligands provides a variety of side chains at the periphery that are directed to one face of the MC (Scheme 1).[8b] The facial differentiation is due to the tetrahedral nature of the carbon and the rotational sense of the MC. 15-MC-5 complexes with Cu^{II} as ring metals have been made with lanthanide ions from La^{III} to Lu^{III} as the encapsulated metal, as well as UO_2^{2+},[5] and Y^{3+}, and the complexes have displayed interesting magnetic properties including single-molecule magnetism.[10e]

Lanthanide(III) ions change significantly in size across the periodic table, with ionic radii that range from 1.160 Å (La^{III}) to 0.977 Å (Lu^{III}) for eight-coordinate ions.[14] The size also changes significantly with the coordination number, changing from 1.100 Å to 1.270 Å for La^{III} as the coordination number increases from 7 to 10.[14] Crown ether chemistry has shown that cations that are matched well in size to the cavity will be bound more strongly and with greater specificity.[15] In addition, the relative size of the cavity impacts how the cation is bound. 18-crown-6 binds potassium exactly in the center of the ring,[16]

Received: April 15, 2011
Published: July 18, 2011

Scheme 1. General Schematic of a $Ln^{III}[15\text{-}MC_{Cu^{II}(N)pheHA}\text{-}5]^{3+}$ Complex[a]

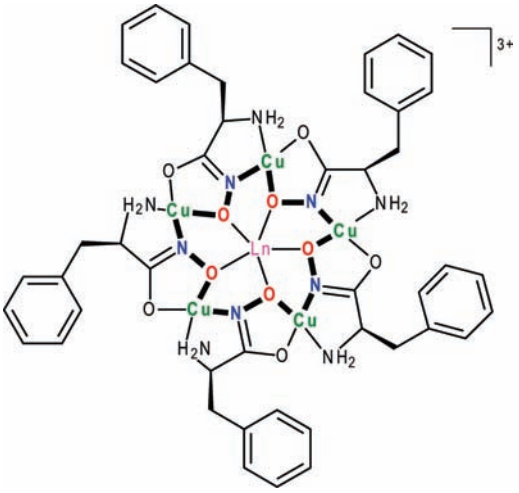

[a] The atoms and bonds that comprise the MC ring are in bold.

while the smaller monobenzo-15-crown-5 cannot encapsulate potassium, but instead forms a "sandwich" complex.[17] 12-MC-4 complexes have been seen to form a similar type of sandwich complex in which a Na-MC-Na-MC-Na structure is formed,[18] while in other cases 12-MC-4 complexes form a 2:1 metal/metallacrown sandwich with potassium and sodium, with a cation bound to both faces of the metallacrown.[19] For larger, more flexible crown ethers, the ligand can wrap around a smaller cation, as seen with dibenzo-30-crown-10 and potassium, or even accommodate two cations as in the case of sodium.[20] Thus, the relative size of the cavity and cation greatly influence the structure adopted by the ring. While 15-MC-5 complexes are not as flexible as crown ethers and the cavities are certainly not large enough to encapsulate two cations, it is very likely that changing the size of the encapsulated lanthanide will impact the metallacrown structure and the position of the lanthanide in the cavity. In developing metallacrowns for use as anion recognition agents, the accessibility of the central cation (whether it lies exactly in the ring or toward one face) and the structure of the metallacrown could be important. It has already been reported that the three-dimensional packing of 15-MC-5 complexes is dependent upon which face the Ln^{III} lies[21] and recent reports suggest that the affinity of guests is directly related to the chosen central lanthanide ion.[22] A recent study has also illustrated that larger Ln^{III} ions have a higher affinity for the 15-metallacrown-5 cavity, with La^{III} forming the most stable species. Furthermore, preparing Ln^{III} 15-MC-5 complexes with the smallest lanthanides is challenging and often leads to unstable molecules.[23]

Herein we report the effect of the lanthanide ion radius on the $Ln^{III}[15\text{-}MC_{Cu^{II}(N)pheHA}\text{-}5]^{3+}$ complex based upon a series of crystal structures of metallacrowns made with phenylalanine hydroxamic acid (pheHA) as the ligand, with nitrate and/or hydroxide as the anion, and where Ln = La^{III}, Ce^{III}, Pr^{III}, Nd^{III}, Sm^{III}, Eu^{III}, Gd^{III}, Tb^{III}, Dy^{III}, Ho^{III}, Er^{III}, Tm^{III}, and Y^{III}. The purpose of this solid-state study of $Ln^{III}[15\text{-}MC_{Cu^{II}(N)pheHA}\text{-}5]^{3+}$ complexes is to help explain the lanthanide preferences for this class of metallacrowns. While correlating quantitatively solid state structures to solution binding affinities is difficult, one may still extract general trends in metallacrown central cation guest binding affinities that are more easily understandable with a clear structural understanding of the macrocyclic structure and how it is influenced by each respective cation. These fundamental structural constraints can be used as a guide to design future metallacrowns with either higher metal affinities or selected coordination number/geometry, and it may lead to the design of $Ln^{III}[15\text{-}MC_{Cu^{II}(N)pheHA}\text{-}5]^{3+}$ complexes with better guest selectivity.

EXPERIMENTAL SECTION

Synthetic Materials. The lanthanide hydrated salts, yttrium nitrate pentahydrate, copper acetate monohydrate, *S*-phenylalanine, *R*-phenylalanine, hydroxylamine hydrochloride, thionyl chloride, and sodium acetate were purchased from Aldrich Chemical and used as received. Deionized water was used in all syntheses, and ACS certified grade potassium hydroxide, methanol, and ethanol were purchased from Fisher Scientific and used as received.

Ligand Syntheses. The synthesis of *S*-phenylalaninehydroxamic acid has also been prepared by our group via a different method.[23]

Preparation of *S*-Phenylalanine Ethyl Ester Hydrochloride. *S*-Phenylalanine (0.05 mol) was stirred in ice-cold ethanol (100 mL) in an ice-bath as $SOCl_2$ (5.6 mL, 0.077 mol) was added dropwise. The ice-bath was removed, and the flask was allowed to reach room temperature and then refluxed for 1.5 h at 78−80 °C. The solvent was removed under reduced pressure leaving a white crystalline solid as the crude product. Crude yield: 11.45 g, 99.7%.

Preparation of *S*-Phenylalaninehydroxamic acid (S-pheHA). $NH_2OH \cdot HCl$ (0.15 mol) was dissolved in methanol (125 mL). KOH (85% purity, 0.15 mol) was dissolved in methanol (50 mL) and added to the $NH_2OH \cdot HCl$ solution, with stirring and under a flow of nitrogen, until the pH was 8−9. KCl precipitated immediately. After 5 min the solution was filtered to remove the KCl. *S*-Phenylalanine ethyl ester hydrochloride (0.05 mol) was dissolved in a minimum of methanol and added to the NH_2OH solution. A solution of KOH (85% purity, 0.093 mol) in methanol was added slowly to the solution, and KCl immediately precipitated. The KOH solution was added until no further precipitate formed, and the solution was slightly basic (~pH 8). The KCl was removed by filtration. The solution was stirred under a flow of nitrogen for 18 h until a large amount of white solid had precipitated. The pure crystalline solid was collected by filtration and washed with methanol and water. Yield: 8.42 g, 93% from *S*-phenylalanine. Analysis for $C_9H_{12}N_2O_2$, found (calculated): C = 59.66 (59.99), H = 6.70 (6.71), N = 15.37 (15.55).

Preparation of *R*-Phenylalanine Ethyl Ester Hydrochloride and *R*-Phenylalaninehydroxamic acid (R-pheHA). To produce R-pheHA a similar procedure was followed except that *R*-phenylalanine was used as the starting reagent. Analysis for $C_9H_{12}N_2O_2$, found (calculated): C = 60.06 (59.99), H = 6.90 (6.71), N = 15.44 (15.55).

Metallacrown Syntheses. *Type 1.* $La(NO_3)_{2.5}[15\text{-}MC_{Cu^{II}(N)R\text{-}pheHA}\text{-}5](OH)_{0.5}$, ***La-1***. R-pheHA (1.0 mmol) was mixed with $Cu(O_2CCH_3)_2 \cdot H_2O$ (1.0 mmol) in 50 mL of water. After 1 h $La(NO_3)_3 \cdot 6H_2O$ (0.20 mmol) was added. After stirring overnight the clear, dark blue solution was filtered. Dark blue crystals were formed after slow evaporation of the solvent. The crystals were collected by vacuum filtration and washed with cold water. Yield 97%. Analysis for $(C_{45}H_{50}N_{10}O_{10}Cu_5La)(NO_3)_{2.5}(OH)_{0.5}(H_2O)_2$, found (calculated): C = 34.84 (34.93), H = 3.55 (3.55), N = 10.93 (11.32). FAB+MS gave $[M \cdot NO_3]^+$ 1407.9 *m/z* and $[M \cdot 2NO_3]^+$ 1469.9 *m/z*.

$Ce(NO_3)_3[15\text{-}MC_{Cu^{II}(N)S\text{-}pheHA}\text{-}5]$, ***Ce-1***. S-pheHA (2.77 mmol), $Cu(O_2CCH_3)_2 \cdot H_2O$ (2.77 mmol), and $Ce(NH_4)_2(NO_3)_6$ (0.55 mmol) were dissolved in 70 mL of water. The solution was stirred for 1 day and then filtered. Slow evaporation of the filtrate at room temperature yielded dark purple crystals. Yield 71%. Analysis for $(C_{45}H_{50}N_{10}O_{10}Cu_5Ce)(NO_3)_3(H_2O)_{10}$, found (calculated): C = 31.68 (31.52), H = 4.15 (4.11), N = 10.59 (10.62).

dx.doi.org/10.1021/ic200740h |*Inorg. Chem.* 2011, 50, 7707–7717

$Pr(NO_3)_2[15\text{-}MC_{Cu^{II}(N)S\text{-}pheHA}\text{-}5](OH)$, ***Pr-1***. S-pheHA (2.77 mmol), $Cu(O_2CCH_3)_2 \cdot H_2O$ (2.77 mmol) and $Pr(NO_3)_3 \cdot 6H_2O$ (0.55 mmol) were dissolved in 70 mL of water. The solution was stirred for 1 day and then filtered. Slow evaporation of the filtrate yielded dark purple crystals. Yield 79%. Analysis for $(C_{45}H_{50}N_{10}O_{10}Cu_5Pr)(NO_3)_2(OH)(H_2O)_6$, found (calculated): C = 33.53 (33.81), H = 3.83 (3.97), N = 10.96 (10.51).

$Nd(NO_3)_{1.5}[15\text{-}MC_{Cu^{II}(N)S\text{-}pheHA}\text{-}5](OH)_{1.5}$, ***Nd-1***. S-pheHA (1.0 mmol) was stirred in 40 mL of water but did not dissolve. $Cu(O_2CCH_3)_2 \cdot H_2O$ (1.0 mmol) and sodium acetate (1.0 mmol) were dissolved in 20 mL of water and added to the ligand mixture, which formed a highly viscous green gel. After 45 min of stirring $Nd(NO_3)_3 \cdot 6H_2O$ (0.20 mmol) was dissolved in 5 mL of water and added to the above gel. After stirring overnight a dark blue solution had formed that was slightly cloudy. Methanol (~3 mL) was added to the mixture, and the solution became clear. After filtering the solution was left to evaporate slowly. Dark blue needle crystals formed, but dried out after all of the solvent was evaporated. The crystals were dissolved in water and recrystallized. The crystals were collected by vacuum filtration and washed with cold water. Yield 38%. Analysis for $(C_{45}H_{50}N_{10}O_{10}Cu_5Nd)(NO_3)_{1.5}(OH)_{1.5}(H_2O)_3$, found (calculated): C = 35.36 (35.43), H = 3.66 (3.80), N = 10.74 (10.56). FAB+MS gave $[M \cdot NO_3]^+$ 1413.6 *m/z* and $[M \cdot 2NO_3]^+$ 1475.0 *m/z*.

$Gd(NO_3)_{1.5}[15\text{-}MC_{Cu^{II}(N)S\text{-}pheHA}\text{-}5](OH)_{1.5}$, ***Gd-1***. S-pheHA (1.0 mmol) was mixed with $Cu(O_2CCH_3)_2 \cdot H_2O$ (1.0 mmol) and $Gd(NO_3)_3 \cdot 6H_2O$ (0.20 mmol) in 40 mL of water. After stirring overnight a clear, dark blue solution had formed. After filtering, the solution was left to evaporate slowly and dark blue crystals formed. The crystals were collected by vacuum filtration and washed with cold water. Yield 84%. Analysis for $(C_{45}H_{50}N_{10}O_{10}Cu_5Gd)(NO_3)_{1.5}(OH)_{1.5}(H_2O)_6$, found (calculated): C = 33.86 (33.94), H = 3.89 (4.02), N = 9.99 (10.11). FAB+MS gave $[M \cdot NO_3]^+$ 1426.9 *m/z* and $[M \cdot 2NO_3]^+$ 1488.9 *m/z*.

$Y(NO_3)[15\text{-}MC_{Cu^{II}(N)S\text{-}pheHA}\text{-}5](OH)_2$, ***Y-1***. S-pheHA (1.0 mmol), $Cu(O_2CCH_3)_2 \cdot H_2O$ (1.0 mmol), and $Y(NO_3)_3 \cdot 5H_2O$ (0.20 mmol) were dissolved in 25 mL of water. The initial mixture had a green color, but upon stirring for approximately 15 minutes, the solution turned dark blue. The solution was then stirred overnight without any color changes. The solution was then filtered to remove a green precipitate, which was subsequently discarded. Slow evaporation of the dark blue filtrate at room temperature yielded dark blue crystals. The crystals were collected by vacuum filtration and washed with cold water. Yield 32%. Analysis for $(C_{45}H_{50}N_{10}O_{10}Cu_5Y)(NO_3)(OH)_2(H_2O)_8$, found (calculated): C = 34.84 (35.15), H = 3.80 (4.46), N = 11.48 (10.02).

Type 2. *$Eu(NO_3)_2[15\text{-}MC_{Cu^{II}(N)S\text{-}pheHA}\text{-}5](OH)$*, ***Eu-2***. S-pheHA (1.0 mmol) was mixed with $Cu(O_2CCH_3)_2 \cdot H_2O$ (1.0 mmol) and $Eu(NO_3)_3 \cdot 6H_2O$ (0.20 mmol) in 20 mL of water and 2 mL of methanol. After 2 h a clear, dark blue solution had formed. After filtering, the solution was left to evaporate slowly and dark blue crystals formed. The crystals were collected by vacuum filtration and washed with cold water. Yield 36%. Analysis for $(C_{45}H_{50}N_{10}O_{10}Cu_5Eu)(NO_3)_2(OH)(H_2O)_6$, found (calculated): C = 33.34 (33.58), H = 3.68 (3.94), N = 10.78 (10.44). FAB+MS gave $[M \cdot NO_3]^+$ 1421.8 *m/z* and $[M \cdot 2NO_3]^+$ 1483.6 *m/z*.

$Tb(NO_3)_2[15\text{-}MC_{Cu^{II}(N)S\text{-}pheHA}\text{-}5](OH)$, ***Tb-2***. S-pheHA (1.0 mmol) was mixed with $Cu(O_2CCH_3)_2 \cdot H_2O$ (1.0 mmol) and $Tb(NO_3)_3 \cdot 6H_2O$ (0.20 mmol) in 20 mL of water and 2 mL of methanol. After 2 h a clear, dark blue solution had formed. After filtering, the solution was left to evaporate slowly and dark blue crystals formed. The crystals were collected by vacuum filtration and washed with cold water. Yield 29%. Analysis for $(C_{45}H_{50}N_{10}O_{10}Cu_5Tb)(NO_3)_2(OH)(H_2O)_{6.5}$, found (calculated): C = 33.21 (33.25), H = 3.76 (3.97), N = 10.20 (10.34). FAB+MS gave $[M \cdot NO_3]^+$ 1428.0 *m/z* and $[M \cdot 2NO_3]^+$ 1489.8 *m/z*.

$Dy(NO_3)_{2.5}[15\text{-}MC_{Cu^{II}(N)S\text{-}pheHA}\text{-}5](OH)_{0.5}$, ***Dy-2***. S-pheHA (1.0 mmol), $Cu(O_2CCH_3)_2 \cdot H_2O$ (1.0 mmol), and $Dy(NO_3)_3 \cdot 5H_2O$ (0.20 mmol) were dissolved in 25 mL of water. The initial mixture had a green color, but upon stirring for approximately 15 minutes, the solution turned dark blue. The solution was then stirred overnight without any color changes. The solution was then filtered to remove a green precipitate, which was subsequently discarded. Slow evaporation of the dark blue filtrate at room temperature yielded dark blue crystals. The crystals were collected by vacuum filtration and washed with cold water. Yield 28%. Analysis for $(C_{45}H_{50}N_{10}O_{10}Cu_5Dy)(NO_3)_{2.5}(OH)_{0.5}(H_2O)_4$, found (calculated): C = 33.80 (33.64), H = 3.81 (3.67), N = 10.48 (10.90).

$Ho(NO_3)_3[15\text{-}MC_{Cu^{II}(N)S\text{-}pheHA}\text{-}5]$, ***Ho-2***. After collecting the crystals of **Ho-3** (see below), the filtrate (consisting of the metallacrown solution that remained when the crystals were collected and additional water from washing the crystals) crystallized after evaporation of most of the solvent. A very small amount of crystals were collected. The yield was not calculated, and an elemental analysis could not be performed. FAB+ MS gave $[M \cdot NO_3]^+$ 1435.0 *m/z* and $[M \cdot 2NO_3]^+$ 1495.8 *m/z*.

$Er(NO_3)_3[15\text{-}MC_{Cu^{II}(N)S\text{-}pheHA}\text{-}5]$, ***Er-2***. S-pheHA (0.5 mmol), $Cu(O_2CCH_3)_2 \cdot H_2O$ (0.5 mmol), and $Er(NO_3)_3 \cdot 5H_2O$ (0.1 mmol) were dissolved in 30 mL of water. The solution was stirred for 1 day and then filtered. Slow evaporation of the filtrate at room temperature yielded dark purple crystals. Yield 75%. Analysis for $(C_{45}H_{50}N_{10}O_{10}Cu_5Er)(NO_3)_3(H_2O)_{8.5}$, found (calculated): C = 31.36 (31.51), H = 3.49 (3.94), N = 9.76 (10.62).

Type 3. *$Sm(NO_3)_2[15\text{-}MC_{Cu^{II}(N)S\text{-}pheHA}\text{-}5](OH)$*, ***Sm(a)-3***. S-pheHA (1.0 mmol) was mixed with $Cu(O_2CCH_3)_2 \cdot H_2O$ (1.0 mmol) and $Sm(NO_3)_3 \cdot 6H_2O$ (0.20 mmol) in 20 mL of water and 2 mL of methanol. After 2 h a clear, dark blue solution had formed. After filtering, the solution was left to evaporate slowly, and dark blue crystals formed. The crystals were collected by vacuum filtration and washed with cold water. Yield 78%. Analysis for $(C_{45}H_{50}N_{10}O_{10}Cu_5Sm)(NO_3)_2(OH)(H_2O)_{7.5}$, found (calculated): C = 32.62 (33.05), H = 3.66 (4.07), N = 10.94 (10.28). ESI-MS gave $[M \cdot NO_3]^{2+}$ 710.4 *m/z* and $[M \cdot 2NO_3]^+$ 1482.8 *m/z*.

$Sm(NO_3)_3[15\text{-}MC_{Cu^{II}(N)R\text{-}pheHA}\text{-}5]$, ***Sm(b)-3***. R-pheHA (1.0 mmol) was mixed with $Cu(O_2CCH_3)_2 \cdot H_2O$ (1.0 mmol) and $Sm(NO_3)_3 \cdot 6H_2O$ (0.20 mmol) in 20 mL of methanol. After 2 h a clear, dark blue solution had formed. After filtering, the solution was left to evaporate slowly, and a glassy film was formed. After dissolving the film in 15 mL of methanol and ~2 mL of water, the resulting solution was left to evaporate slowly. Dark blue crystals were formed. The crystals were dissolved in 10 mL of methanol and ~0.5 mL of water, and the solution was left to evaporate slowly. Dark blue crystals were formed when ~3 mL of the liquor remained. The crystals were collected by vacuum filtration and washed with cold water. Yield 83%. Analysis for $(C_{45}H_{50}N_{10}O_{10}Cu_5Sm)(NO_3)_3(H_2O)_{4.5}$, found (calculated): C = 33.19 (33.24), H = 3.69 (3.66), N = 11.04 (11.20).

$Sm(NO_3)_{1.5}[15\text{-}MC_{Cu^{II}(N)S\text{-}pheHA}\text{-}5](OH)_{1.5}$, ***Sm(c)-3***. S-pheHA (1.0 mmol), $Cu(O_2CCH_3)_2 \cdot H_2O$ (1.0 mmol) and $Sm(NO_3)_3 \cdot 6H_2O$ (0.20 mmol) were dissolved in 20 mL of water and 2 mL of methanol. The solution was stirred for 1 day and then filtered. Slow evaporation of the filtrate at room temperature yielded dark purple crystals. Yield 78%. Analysis for $(C_{45}H_{50}N_{10}O_{10}Cu_5Sm)(NO_3)_{1.5}(OH)_{1.5}(H_2O)_{8.5}$, found (calculated): C = 32.62 (33.14), H = 3.66 (4.23), N = 10.94 (9.88).

$Eu(NO_3)_2[15\text{-}MC_{Cu^{II}(N)S\text{-}pheHA}\text{-}5](OH)$, ***Eu-3***. S-pheHA (1.0 mmol), $Cu(O_2CCH_3)_2 \cdot H_2O$ (1.00 mmol), and $Eu(NO_3)_3 \cdot 5H_2O$ (0.20 mmol) were dissolved in 20 mL of water and 2 mL of methanol. The solution was stirred for 1 day and then filtered. Slow evaporation of the filtrate at room temperature yielded dark purple crystals. Yield 36.5%. Analysis for $(C_{45}H_{50}N_{10}O_{10}Cu_5Eu)(NO_3)_2(OH)(H_2O)_6$, found (calculated): C = 33.34 (33.58), H = 3.68 (3.94), N = 10.78 (10.44).

$Gd(NO_3)_3[15\text{-}MC_{Cu^{II}(N)S\text{-}pheHA}\text{-}5]$, ***Gd(a)-3***. S-pheHA (1.00 mmol), $Cu(O_2CCH_3)_2 \cdot H_2O$ (1.00 mmol), and $Gd(NO_3)_3 \cdot 6H_2O$ (0.20 mmol) were dissolved in 40 mL of water. The solution was stirred for 1 day and then filtered. Slow evaporation of the filtrate at room temperature yielded dark purple crystals. Yield 84.6%. Analysis for $(C_{45}H_{50}N_{10}O_{10}Cu_5Gd)(NO_3)_3(H_2O)_4$, found (calculated): C = 33.86 (33.28), H = 3.89 (3.60), N = 9.99 (11.21).

dx.doi.org/10.1021/ic200740h |*Inorg. Chem.* 2011, 50, 7707–7717

$Gd(NO_3)_2$[15-$MC_{Cu^{II}(N)R\text{-}pheHA}$-5](OH), ***Gd(b)-3***. R-pheHA (1.0 mmol), $Cu(O_2CCH_3)_2 \cdot H_2O$ (1.0 mmol), and $Gd(NO_3)_3.6H_2O$ (0.20 mmol) were dissolved in 25 mL of water and 5 mL of methanol. The initial mixture had a green color, but upon stirring for approximately 5 min, the solution turned dark blue. The solution was then stirred overnight without any color changes. The solution was then filtered and no green precipitate was recovered. Slow evaporation of the dark blue filtrate at room temperature yielded dark blue crystals. The crystals were collected by vacuum filtration and washed with cold water. Yield 42%. Analysis for $(C_{45}H_{50}N_{10}O_{10}Cu_5Gd)(NO_3)_2(OH)(H_2O)_6$, found (calculated): C = 33.23 (33.47), H = 3.93 (3.93), N = 10.64 (10.41).

$Dy(NO_3)_2$[15-$MC_{Cu^{II}(N)S\text{-}pheHA}$-5](OH), ***Dy-3***. S-pheHA (1.0 mmol), $Cu(O_2CCH_3)_2 \cdot H_2O$ (1.0 mmol), and $Dy(NO_3)_3 \cdot 5H_2O$ (0.20 mmol) were dissolved in 25 mL of water and 5 mL of methanol. The initial mixture had a green color, but upon stirring for approximately 5 min, the solution turned dark blue. The solution was then stirred overnight without any color changes. The solution was then filtered, and no green precipitate was recovered. Slow evaporation of the dark blue filtrate at room temperature yielded dark blue crystals. The crystals were collected by vacuum filtration and washed with cold water. Yield 39%. Analysis for $(C_{45}H_{50}N_{10}O_{10}Cu_5Dy)(NO_3)_2(OH)(H_2O)_{4.5}$, found (calculated): C = 33.54 (33.92), H = 3.59 (3.80), N = 11.18 (10.55).

$Ho(NO_3)_2$[15-$MC_{Cu^{II}(N)S\text{-}pheHA}$-5](OH), ***Ho-3***. S-pheHA (1.0 mmol) was mixed with $Cu(O_2CCH_3)_2 \cdot H_2O$ (1.0 mmol) and $Ho(NO_3)_3 \cdot 6H_2O$ (0.20 mmol) in 20 mL in water and 2 mL in methanol. After 2 h a clear, dark blue solution had formed. After filtering, the solution was left to evaporate slowly, and dark blue crystals formed. The crystals were collected by vacuum filtration and washed with cold water. The crystals were collected by vacuum filtration and washed with cold water. Yield 59%. Analysis for $(C_{45}H_{50}N_{10}O_{10}Cu_5Ho)(NO_3)_2(OH)(H_2O)_{12.5}$, found (calculated): C = 30.78 (31.07), H = 3.90 (4.40), N = 10.08 (9.66). FAB+MS gave $[M \cdot NO_3]^+$ 1435.0 *m*/*z* and $[M \cdot 2NO_3]^+$ 1495.8 *m*/*z*.

$Tm(NO_3)_3$[15-$MC_{Cu^{II}(N)S\text{-}pheHA}$-5], ***Tm-3***. S-pheHA (1.0 mmol) was mixed with $Cu(O_2CCH_3)_2 \cdot H_2O$ (1.0 mmol) and $Tm(NO_3)_3 \cdot 6H_2O$ (0.20 mmol) in 40 mL of methanol. After stirring overnight the clear, dark blue solution was filtered, and left to evaporate slowly. After a few days some green powdery solid had formed in the flask. After removing the solid by filtration, the remaining blue solution was again left to evaporate slowly. A small amount of dark blue crystals was formed after slow evaporation of the solvent, along with additional green powdery solid. A single crystal X-ray diffraction pattern was immediately measured because of rapid decomposition of the crystals. A percent yield was not calculated, and an elemental analysis could not be performed.

Physical Methods. X-ray Crystallography. A crystal of each sample was mounted on a standard Bruker SMART CCD-based X-ray diffractometer equipped with a LT-2 low temperature device and Mo-target X-ray tube (λ = 0.71073 Å) operated at 2000 W power (50 kV, 40 mA). Additional details are provided in Supporting Information, Tables S1−S3 and in the individual CIF file for each sample.

RESULTS

General Description of the X-ray Crystal Structures. Crystal structures of $Ln^{III}[15\text{-}MC_{Cu^{II}(N)pheHA}\text{-}5]^{3+}$ where Ln = La^{III}, Ce^{III}, Pr^{III}, Nd^{III}, Sm^{III}, Eu^{III}, Gd^{III}, Tb^{III}, Dy^{III}, Ho^{III}, Er^{III}, Tm^{III}, and Y^{III}have been completed. Though Y^{III} is not a lanthanide ion, we have included its chemistry since it has the same charge and a very similar ionic radius to many of the lanthanide ions (Supporting Information, Table S4). The anions (nitrate and hydroxide) have been omitted from the general chemical formula since the number of each particular anion can vary, and the coordination mode of the anions can vary from structure to structure. The number and the nature of the coordination of the anions is imperative to the individual structure classes (i.e., Types 1−3 described below). How the anions influence the solid state features are explained in the descriptions below; however, the anions have been omitted from the formula since the stoichiometries are not consistent across all structures. It is our belief that within each structural category that accounts for the influence of the anion, we can treat the structures of the cations independently. Because of the number of crystal structures (20) and the fact that many of the structures have been previously reported in full detail,[7,8b,21] descriptions of each individual structure will only be included in the Supporting Information. In addition, the focus of this paper is not the individual structures, but instead how the central ion affects the metallacrown structure. Thus, below is a general description of the basic $Ln^{III}[15\text{-}MC_{Cu^{II}(N)pheHA}\text{-}5]^{3+}$ motif and a brief description of the three Types (i.e., classes) of $Ln^{III}[15\text{-}MC_{Cu^{II}(N)pheHA}\text{-}5]^{3+}$ structures. In addition, structural figures will only be presented for representatives of each metallacrown Type. Figures for each crystal structure may be found in the Supporting Information, Figures S1−S41. Table 1 contains a summary of the features of each metallacrown structure.

While the number of the metallacrowns per unit cell can vary (one, two, or four), the basic structure of each metallacrown complex is very similar, with the phenyl groups of the ligand oriented at the periphery of the planar, disk-shaped molecule. The general crystal structures of $Ln^{III}[15\text{-}MC_{Cu^{II}(N)pheHA}\text{-}5]^{3+}$ complexes have been reported previously[7,8b,21] but here we provide a complete description of all nitrate/hydroxide metallacrown structures. The phenyl groups are all oriented to the same face of the metallacrown creating a hydrophobic "pocket"; however, the exact orientation of the phenyl groups can differ depending on the crystal structure. Differing numbers of phenyl groups can be directly curled underneath the face of the metallacrown or "splayed", pointing out from the periphery of the metallacrown, while still directed toward the hydrophobic face. Anions or solvent molecules may be bound to the central lanthanide ion or act as axial ligands to the ring copper(II) ions. The lanthanides are 8 or 9 coordinate in these metallacrowns, with 5 oxime oxygen donors from the metallacrown and 3 or 4 anion/solvent donors. The lanthanide typically lies slightly out of the plane of the metallacrown, and all of the metallacrowns are slightly ruffled. X-ray crystallographic parameters for all structures are given in Supporting Information, Tables S1−S3 with further details found in the CIF files of each individual compound (Supporting Information).

The 20 reported structural models can be divided into three categories based on the similarity of the crystal structures. Structures **La-1**, **Ce-1**, **Pr-1**, **Nd-1**, **Gd-1**, and **Y-1** have been grouped together as "Type 1". Figures of **La-1** serve as a representation of Type 1 metallacrowns (Figure 1 and Supporting Information, Figures S1−S5), and additional figures of Type 1 metallacrowns may be found in the Supporting Information, Figures S6−S10. These metallacrowns typically interact through their hydrophilic faces through bridging water molecules or nitrate anions. For all structures (the exception being **Gd-1**), two phenyl groups are curled underneath the hydrophobic face and three phenyl groups are splayed to the outside. More importantly, two metallacrowns in each Type 1 structure interact via their phenyl groups to form an offset dimer with a hydrophobic pocket (Supporting Information, Figures S3−S4), and the Ln^{III} of each metallacrown *does not* bind a nitrate anion in a bidentate fashion in the hydrophobic pocket. Moreover, the Ln^{III} in each Type 1 structure lies out of the oxime oxygen mean plane of the metallacrown toward the hydrophilic face.

Table 1. Feature Comparison of Type 1, Type 2, and Type 3 $Ln^{III}[15\text{-}MC_{Cu^{II}(N)pheHA}\text{-}5]^{3+}$ Complexes

structure	number of curled phenyl groups	Ln^{III} coordination number	Ln^{III} distance to OMP (Å)	to which faces does the Ln^{III} lie	does the Ln^{III} bind a bidentate NO_3^- on the hydrophobic face?	do the MCs form a hydrophobic pocket?	$Ln^{III}-Ln^{III}$ hydrophilic distance (Å)	$Ln^{III}-Ln^{III}$ hydrophobic distance (Å)
La-1	2	9	0.68	hydrophilic	no	yes	8.89	12.03
Ce-1	2	9	0.65	hydrophilic	no	yes	10.20	12.05
Pr-1	2	9	0.62	hydrophilic	no	yes	8.88	11.94
Nd-1	2	8	0.35 (Nd1) and 0.27 (Nd2)	hydrophilic	no	yes	8.94 (Nd1−Nd2)	11.70 (Nd1−Nd1) and 11.24 (Nd2−Nd2)
Gd-1	2 and 1 or 2	8	0.31 (Gd1) and 0.35 (Gd2)	hydrophilic	no	yes	9.17 (Gd1−Gd2)	11.10 (Gd1−Gd1) and 11.36 (Gd2−Gd2)
Y-1	2	8	0.24 (Y1) and 0.32 (Y2)	hydrophilic	no	yes	9.21 (Y1−Y2)	11.03 (Y1−Y1) and 11.41 (Y2−Y2)
Eu-2	4 (Type A) and 5 (Type B)	8	0.34 (Eu1, Type A) and 0.20 (Eu2, Type B)	hydrophobic	yes	yes	8.36 (Eu1−Eu1) and 6.74 (Eu2−Eu2)	11.55 (Eu1−Eu2)
Tb-2	4 (Type A) and 5 (Type B)	8	0.31 (Tb2, Type A) and 0.20 (Tb1, Type B)	hydrophobic	yes	yes	8.37 (Tb2−Tb2) and 6.69 (Tb1−Tb1)	11.54 (Tb1−Tb2)
Dy-2	4 (Type A) and 5 (Type B)	8	0.28 (Dy2, Type A) and 0.19 (Dy1, Type B)	hydrophobic	yes	yes	8.36 (Dy2−Dy2) and 6.64 (Dy1−Dy1)	11.55 (Dy1−Dy2)
Ho-2	4 (Type A) and 5 (Type B)	8	0.29 (Ho1, Type A) and 0.19 (Ho2, Type B)	hydrophobic	yes	yes	8.34 (Ho1−Ho1) and 6.61 (Ho2−Ho2)	11.50 (Ho1−Ho2)
Er-2	4 (Type A) and 5 (Type B)	8	0.27 (Er1, Type A), 0.32 (Er4, Type A), 0.17 (Er2, Type B), and 0.21 (Er3, Type B)	hydrophobic	yes	yes	8.36 (Er1−Er4) and 6.61 (Er2−Er3)	11.45 (Er1−Er3) and 11.55 (Er2−Er4)
Sm(a)-3	3	8	0.20	hydrophobic	yes	no	9.53	14.33
Sm(b)-3	3	8	0.20	hydrophobic	yes	no	9.52	14.33
Sm(c)-3	3	8	0.10 (Sm1) and 0.02 (Sm2)	hydrophobic	yes	no	9.14 (Sm1−Sm2)	14.53 (Sm1−Sm1) and 14.41 (Sm2−Sm2)
Eu-3	3	8	0.20	hydrophobic	yes	no	9.55	14.37
Gd(a)-3	3	8	0.19	hydrophobic	yes	no	9.54	14.35
Gd(b)-3	3	8	0.20	hydrophobic	yes	no	9.52	14.33
Dy-3	3	8	0.19	hydrophobic	yes	no	9.51	14.33
Ho-3	3	8	0.20	hydrophobic	yes	no	9.53	14.32
Tm-3	3	8	0.19	hydrophobic	yes	no	9.52	14.32

dx.doi.org/10.1021/ic200740h |*Inorg. Chem.* 2011, 50, 7707–7717

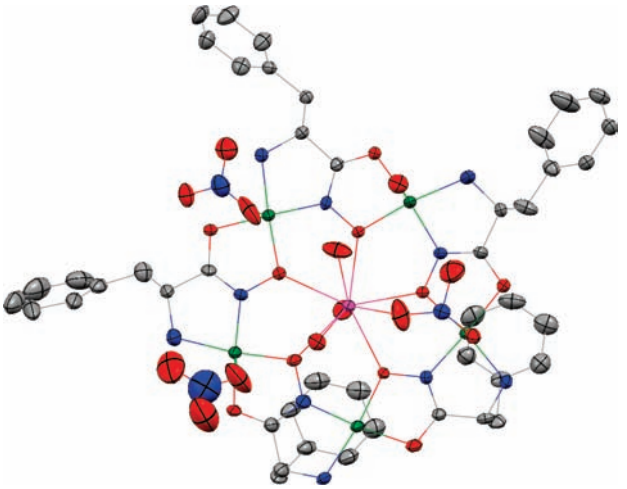

Figure 1. X-ray crystal structure of **La-1**, top view. Hydrogen atoms and lattice solvent/anions have been omitted for clarity. Color scheme: gray, carbon; red, oxygen; blue, nitrogen; green, Cu^{II}; magenta, La^{III}. Thermal ellipsoids displayed at 50% probability.

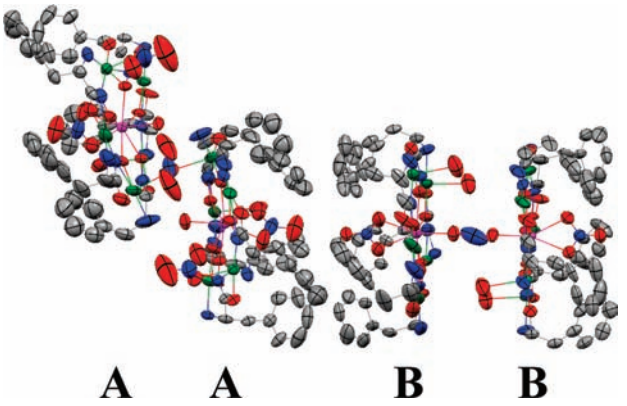

Figure 2. X-ray crystal structure of **Eu-2**, with two unique metallacrowns. Hydrogen atoms and lattice solvent/anions have been omitted for clarity. Color scheme: gray, carbon; red, oxygen; blue, nitrogen; green, Cu^{II}; magenta, Eu^{III}. Thermal ellipsoids displayed at 50% probability.

Structures **Eu-2**, **Tb-2**, **Dy-2**, **Ho-2**, and **Er-2** have been collected together as "Type 2". Figures of **Eu-2** serve as a representation of Type 2 metallacrowns (Figure 2 and Supporting Information, Figures S11−S14), and additional figures of Type 2 metallacrowns may be found in the Supporting Information, Figures S15−S31. These metallacrowns interact through their hydrophilic faces through a bridging nitrate or methanol molecule (**Ho-2** only). In addition, two metallacrowns interact via their phenyl groups to form a dimer with a hydrophobic pocket, and in this dimer the metallacrown molecules are nearly eclipsed (Supporting Information, Figures S13 and S14). Moreover, the Ln^{III} of each metallacrowns *does* bind a nitrate anion in a bidentate fashion inside the hydrophobic pocket. Also, the Ln^{III} lies out of the oxime oxygen mean plane toward the hydrophobic pocket. Furthermore, two types of metallacrowns exist in each Type 2 structure and can be further subcategorized as Type 2A and Type 2B. The Type 2A metallacrowns have a water coordinated to the Ln^{III} on the hydrophilic face, have four phenyl groups curled underneath the hydrophobic face, and have one phenyl group splayed to the outside (Supporting Information, Figure S11). The Type 2B metallacrowns have a nitrate bound in a monodentate fashion to the Ln^{III} on the hydrophilic face, and the nitrate forms a bridge to an adjacent metallacrown (Supporting Information, Figure S12). These molecules have five phenyl groups curled underneath the hydrophobic face; hence no phenyl groups are splayed to the outside. Interestingly, for the Type 2B metallacrowns, the Ln^{III} ions are closer to the oxime oxygen mean plane than the Ln^{III} ions in Type 2A metallacrowns.

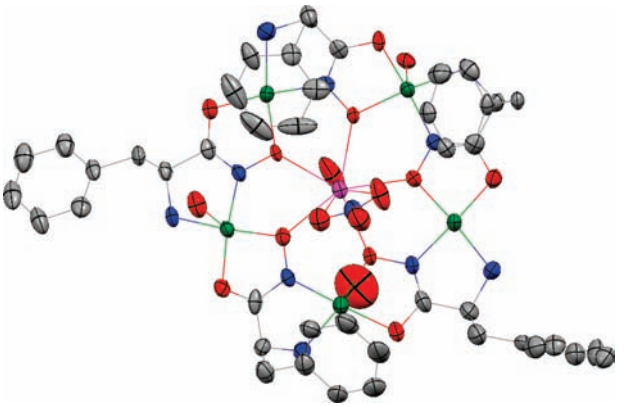

Figure 3. X-ray crystal structure of **Sm(a)-3**. Hydrogen atoms and lattice solvent/anions have been omitted for clarity. Color scheme: gray, carbon; red, oxygen; blue, nitrogen; green, Cu^{II}; magenta, Sm^{III}. Thermal ellipsoids displayed at 50% probability.

Structures **Sm(a)-3**, **Sm(b)-3**, **Sm(c)-3**, **Eu-3**, **Gd(a)-3**, **Gd(b)-3**, **Dy-3**, **Ho-3**, and **Tm-3** have been grouped together as "Type 3". The figure of **Sm(a)-3** serves as a representation of Type 3 metallacrowns (Figure 3), and additional figures of Type 3 metallacrowns may be found in the Supporting Information, Figures S32−S41. These structures do not interact via their hydrophilic or hydrophobic faces as in Type 1 and Type 2. Instead, the Type 3 metallacrowns form one-dimensional helices (Supporting Information, Figures S34 and S40). The Ln^{III} of each metallacrown binds a nitrate anion in a bidentate fashion on the hydrophobic face, and the Ln^{III} lies out of the oxime oxygen mean plane toward the hydrophobic face. In addition, each metallacrown has three phenyl groups curled underneath the hydrophobic face and two phenyl groups splayed to the outside. The structure of **Sm(c)-3** deserves a few more comments. This is the only Type 3 structure with the space group $P2_1$; all other Type 3 structures have a space group of either $P4_1$ or $P4_3$. In addition, **Sm(c)-3** is the only known structure of $Ln^{III}[15\text{-}MC_{Cu^{II}(N)pheHA}\text{-}5]^{3+}$ with a nitrate bound in a bidentate fashion to the Ln^{III} on the hydrophilic face. Though this nitrate is at 50/50 occupancy on both the hydrophobic or hydrophilic faces of the MC, the presence of the nitrate on the hydrophilic face distinguishes this structure from the other Type 3 metallacrowns.

DISCUSSION

The lanthanides from La^{III} to Lu^{III} vary in ionic radius from 1.160 to 0.977 Å when they are eight-coordinate, and the ionic radius increases by ~0.06 Å each time the coordination number increases (Supporting Information, Table S4).[14] The 20 crystal structures presented here include eight-coordinate lanthanides Nd^{III}, Sm^{III}, Eu^{III}, Gd^{III}, Tb^{III}, Dy^{III}, Ho^{III}, Er^{III}, Tm^{III}, and Y^{III}, and nine-coordinate La^{III}, Ce^{III}, and Pr^{III}. This gives an

dx.doi.org/10.1021/ic200740h |*Inorg. Chem.* 2011, 50, 7707–7717

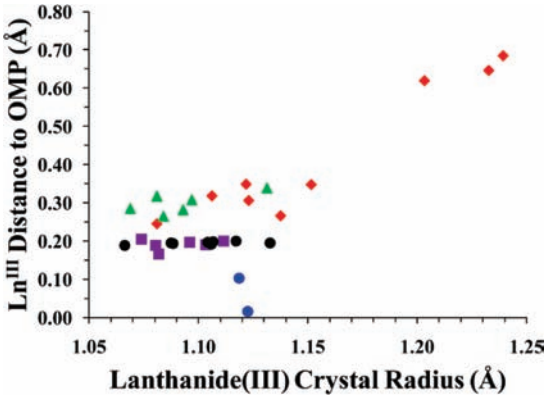

Figure 4. Plot of lanthanide(III) crystal radius versus the Ln^{III} distance to the oxygen mean plane (OMP). The data are grouped by structure type: Type 1 (red solid diamonds), Type 2A (green solid triangles), Type 2B (purple solid squares), Type 3 (black solid circles), and Sm(c)-3 (blue solid circles).

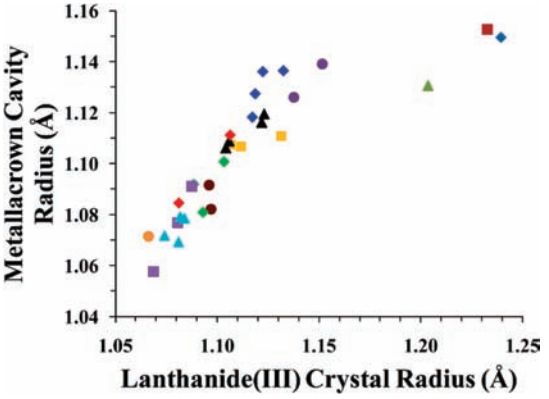

Figure 5. Plot of lanthanide(III) crystal radius versus metallacrown cavity radius. The data are grouped by lanthanide(III) ion identity: La^{III} (light blue solid diamonds), Ce^{III} (reddish brown solid squares), Pr^{III} (light green solid triangles), Nd^{III} (purple solid circles), Sm^{III} (blue solid diamonds), $Eu;^{III}$ (yellow solid squares), Gd^{III} (black solid triangles), Tb^{III} (brown solid circles), Dy^{III} (green solid diamonds), Ho^{III} (purple solid squares), Er^{III} (light blue solid triangles), Tm^{III} (orange solid circles), and Y^{III} (red solid diamonds).

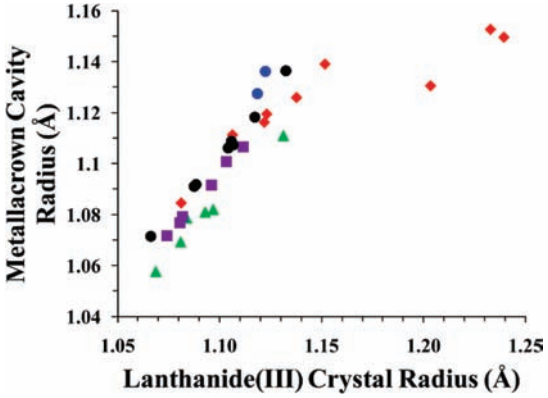

Figure 6. Plot of lanthanide(III) crystal radius versus metallacrown cavity radius. The data are grouped by structure type: Type 1 (red solid diamonds), Type 2A (green solid triangles), Type 2B (purple solid squares), Type 3 (black solid circles), and Sm(c)-3 (blue solid circles).

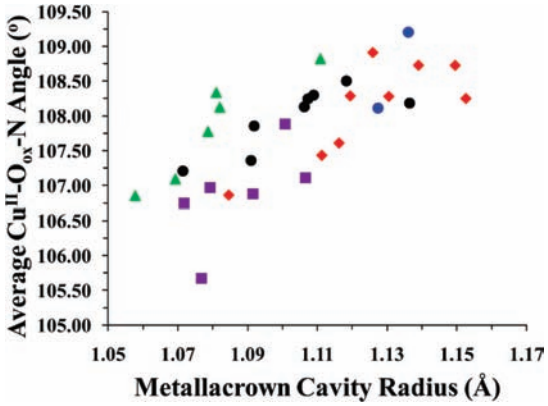

Figure 7. Plot of metallacrown cavity radius versus the average Cu^{II}–oxime oxygen (O_{ox})–nitrogen bond angle. The data are grouped by structure type: Type 1 (red solid diamonds), Type 2A (green solid triangles), Type 2B (purple solid squares), Type 3 (black solid circles), and Sm(c)-3 (blue solid circles).

approximate ionic radii range of 0.994 Å (Tm^{III}) to 1.216 Å (La^{III}). Given that the specificity of the host for a guest typically shows a dependence on a good match between the cavity size and guest size, it seems likely that changing the encapsulated metal in a metallacrown will have an effect on the metallacrown as a better or worse fit will be observed in the crystal structure. Thus plots were constructed to help determine the correlation between the different metallacrown structural features. The numerical parameters for Figures 4–8 and Supporting Information, Figures S42–S46 can be found in Supporting Information, Table S5.

The lanthanide ion crystal radius is determined from the crystal structures by taking the average Ln^{III}–O_{oxime} distance and subtracting the oxygen radius. The lanthanide has oxygen donors that include the five oxime donors in the metallacrown ring, as well as water, hydroxide, and nitrate ligands that vary from structure to structure. Because of this variation, calculating the radius from an average of *all* of the Ln^{III}–O distances with a fixed value for the oxygen radius would not be accurate. Instead, different radii for each oxygen type would have to be used for each Ln^{III}–O bond, thus complicating the calculation. In addition, ensuring a correct value for the oxygen radius of each type of oxygen donor would not be possible. However, for each structure, the five oxime oxygen donors to the central lanthanide ion are consistent; therefore, a value for the lanthanide crystal radius for each metallacrown was calculated using the average Ln^{III}–O_{oxime} distance and then subtracting an estimated value of 1.30 Å for the oxime oxygen radius.

It was expected that as the lanthanide crystal radius increased the lanthanide would be less able to fit in the cavity provided by the five oxime oxygens; thus, the Ln^{III} ion would lie further from the mean plane made by those oxygen atoms. The oxime oxygen mean plane (OMP) values were calculated using the SHELXTL software program. A chart showing this "deviation" from the plane plotted against the lanthanide crystal radius for each metallacrown is shown in Supporting Information, Figure S42, where the data points are shown by central ion type. In addition, Figure 4 shows the data plot by type of metallacrown. For each metallacrown, if there is no nitrate anion bound to the lanthanide on either face, the lanthanide lies toward the hydrophilic face

dx.doi.org/10.1021/ic200740h |*Inorg. Chem.* 2011, 50, 7707–7717

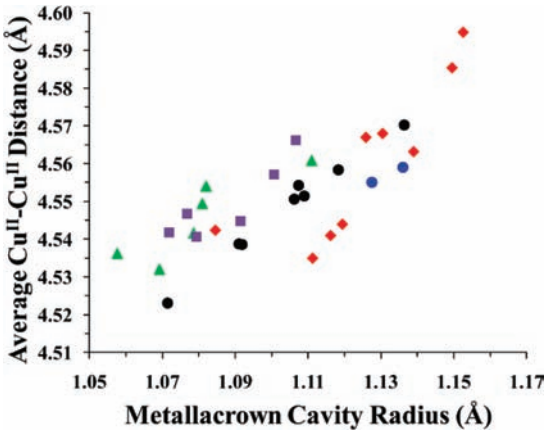

Figure 8. Plot of metallacrown cavity radius versus the average Cu(II)−Cu(II) distance. The data are grouped by structure type: Type 1 (red solid diamonds), Type 2A (green solid triangles), Type 2B (purple solid squares), Type 3 (black solid circles), and Sm(c)-3 (blue solid circles).

(Ce^{III}, Nd^{III}, Gd^{III}, and Y^{III}, all Type 1). If there is one nitrate anion bound to the lanthanide, it lies toward the face that has the nitrate bound. For La^{III} and Pr^{III} (both Type 1), the nitrate is bound in a monodentate fashion on the hydrophilic face and the Ln^{III} lies to the hydrophilic face. For all Type2A and Type 3 metallacrowns, the Ln^{III} binds a nitrate in a bidentate fashion on the hydrophobic face, and the Ln^{III} lies toward the hydrophobic face. Finally, when nitrate anions are bound to both faces (all Type 2B MCs), the lanthanide lies close to the oxime oxygen plane, but toward the face that has the bidentate nitrate. It can be seen from Supporting Information, Figure S42 that there is a general trend for the lanthanide to deviate further from the OMP as the radius increases; however, it is not a strong trend, and it is certainly not a linear relationship. The Sm^{III} value for Sm2 of **Sm(c)-3** strongly differs from the overall trend. The Sm^{III} practically resides in the OMP (Table 1). The Sm2 of **Sm(c)-3** has a bidentate nitrate that is disordered over both the hydrophobic and the hydrophilic faces at 50% occupancy on both faces; thus, the Sm^{III} likely resides in the OMP because of the disordered nitrate which "pulls" the Sm^{III} to the face on which the nitrate is bound. This Sm^{III} is clear evidence that the central ion has a tendency to lie toward the face that contains the nitrate. In addition, there is a large gap between the three ions La^{III}, Pr^{III}, and Ce^{III} and the rest of the ions starting with Nd^{III}. There is a large increase in both the lanthanide crystal radius and the distance from the OMP on moving from Pr^{III} to Nd^{III}. This gap is due to the much larger radius for La^{III}, Pr^{III}, and Ce^{III} which, unlike all of the other metallacrowns, are nine-coordinate. The size of the lanthanide increases with an increase in coordination number; hence, the La^{III}, Pr^{III}, and Ce^{III} radii are larger than would be expected if they were eight-coordinate. The increase in the lanthanide crystal radius causes the ions to reside much farther from the OMP than the other central ions. On looking at the data when it is grouped by type of metallacrown it becomes clear that within each type there is a clear trend that the lanthanide crystal radius does not affect the distance of the lanthanide from the OMP. In all eight-coordinate structures (excluding **Sm(c)-3**), the data shows a nearly straight line for the metallacrowns. In these instances, the lanthanide cavity radius increase does not increase the distance of the lanthanide to OMP.

Scheme 2. Calculation of the Metallacrown Cavity Radius (CR) from the Average Oxime Oxygen (O_{ox})−Oxime Oxygen Distance in a Metallacrown

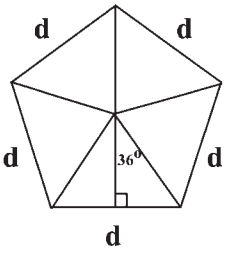

$$d = \frac{\Sigma O_{ox} - O_{ox}}{5}$$

$$R = \frac{d}{2\sin 36^{o}}$$

$$CR = R - R_{ox}$$

Moreover, the three nine-coordinate Ln^{III} (La^{III}, Ce^{III}, and Pr^{III}) are grouped together in the upper right-hand corner of the plot. Thus, the Ln^{III} distance to the OMP seems to be dictated by the coordination number of the lanthanide and controlled by the nature of the bound nitrate (Type 1 C.N. = 8, no nitrate; Type 2A, one bidentate nitrate; Type 2B, one bridging nitrate and one bidentate nitrate; Type 3, one bidentate nitrate).

Another possibility for the lack of change in the distance from the OMP with increasing lanthanide crystal radius might be that the metallacrown cavity changes size to accommodate lanthanides of such different radii. The cavity radius of a metallacrown is calculated by defining a regular pentagon with sides equal to the average O_{oxime}−O_{oxime} distance in the metallacrown. The distance from the center to a corner of the pentagon minus the oxime oxygen radius equals the cavity radius (Scheme 2). Plots of lanthanide crystal radius versus metallacrown cavity radius are shown in Figures 5 and 6. It is apparent from these plots that there is a relatively good correlation between the lanthanide radius and the cavity radius. When separated by type, clear linear relationships are seen with the exception of the nine-coordinate Type 1 structures. Thus, as the lanthanide crystal radius increases, the metallacrown cavity radius increases to accommodate the larger ion. However, it seems that the metallacrown cannot expand its cavity infinitely to fit the largest Ln^{III} ions. In general, for a given eight-coordinate lanthanide radius, Types 1, 2B, and 3 have similar metallacrown cavity sizes, while Type 2A has the smallest metallacrown cavity.

Given that the cavity radius can increase from 1.058 Å (Ho^{III}) to 1.153 Å (Ce^{III}), it seems that it should be possible for the smaller lanthanides to fit completely in the cavity and be positioned directly in the OMP. On the contrary, even the smallest lanthanides are positioned at least 0.19 Å (Tm^{III}) from the OMP, and so it is not possible for a lanthanide to lie exactly in the mean plane made by the donor oxygen atoms (Supporting Information, Figure S43). [The exception is the **Sm(c)-3** with the disordered nitrate.] When the geometry of the oxime oxygen atoms is taken into consideration, this conundrum is quite understandable. The O_{oxime}−N_{oxime} and O_{oxime}−Cu^{II} bonds in the metallacrown lie roughly in the plane of the metallacrown. For a tetrahedral oxygen atom, the two remaining nonbonding pairs of electrons must be positioned above and below the plane of the metallacrown. For the O_{oxime}−Ln^{III} bond to lie in the OMP would therefore be very unfavorable, and thus the lanthanide will lie out of the plane of the metallacrown.

For the eight-coordinate lanthanide ions, Types 1, 2B, and 3 have similar metallacrown cavity sizes, while Type 2A has the smallest metallacrown cavity. Thus the lanthanides of Types 1, 2B, and 3 should have a similar distance to the OMP, and lanthanides

dx.doi.org/10.1021/ic200740h |*Inorg. Chem.* 2011, 50, 7707–7717

Scheme 3. As the Cu^{II}−Oxime Oxygen (O_{ox})−Nitrogen Angle Increases, the Oxygen Atoms Move Outwards and the Metallacrown Cavity Size Increases

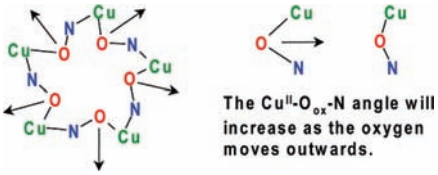

of Type 2A should have the greatest distance to the OMP. A larger cavity should encapsulate more of the lanthanide; thus, the lanthanide will become closer to the metallacrown. Types 2B and 3 have similar distances to the OMP (∼0.20 Å), but Type 1 lanthanides are nearly 0.10 Å greater away at 0.30 Å (Figure 4 and Supporting Information, Figure S43). In Type 2B and 3, the lanthanide binds either one nitrate on either face (Type 2B) or one nitrate on the hydrophobic face (Type 3); however, in eight-coordinate lanthanide Type 1 structures no nitrates are bound to the lanthanide, only water solvent molecules. This structural difference may lead to the different OMP distances for Types 2B and 3 versus Type 1. Furthermore, lanthanides of Type 2A should reside as close to the OMP as Type 2B and 3 since the lanthanides also coordinate a nitrate. However, as seen in Figure 4 and Supporting Information, Figure S43, this is not the case. Type 2A structures have the smallest metallacrown cavity radii so the lanthanides cannot approach the OMP as close as Types 2B and 3, but they do approach the OMP as close as eight-coordinate lanthanides of Type 1 (∼0.30 Å).

It has been shown that the cavity radius increases in size as the lanthanide radius increases. For the cavity size to increase, the oxime oxygens must move and become further away from each other. To determine how this occurs, different metrical parameters in the metallacrown were measured. If the metallacrown cavity expands by simply moving the oxygens "outwards", while keeping them in the same plane, then the Cu^{II}−O_{oxime}−N_{oxime} angle would increase as the lanthanide radius, and thus the cavity radius increases (Scheme 3). The five Cu^{II}−O_{oxime}−N_{oxime} angles in each metallacrown were measured, and the mean value for each metallacrown was plotted against the metallacrown cavity radius (Figure 7). The plot shows a general trend for every type that the Cu^{II}−O_{oxime}−N_{oxime} increases as the metallacrown cavity radius increases. However, this does not prove that the oxime oxygen atoms move only "outwards" and continue to lie in approximately the same plane. Measuring the deviation of each oxime oxygen to the oxime oxygen mean plane will give some insight into the planarity of the metallacrown. The average deviation of the five oxime oxygen atoms to the OMP was plotted against the metallacrown cavity radius to determine whether the oxygen atoms must move further out of the plane for the cavity to expand (Supporting Information, Figure S44). The oxime oxygen deviation to the OMP for Types 2A and 3 remain relatively constant as the metallacrown cavity radius increases; however, there is a very slight decrease to the oxime oxygen deviation to the OMP as the metallacrown cavity radius increases. This implies that the metallacrown becomes less ruffled, and more planar as the metallacrown cavity radius increases. The oxime oxygen atoms move "outwards" and become more planar at the same time. For Type 2B, there is virtually no change in the O_{oxime}−OMP distance as the metallacrown cavity radius increases (the

Scheme 4. Oxime Oxygen (O_{ox})−Cu^{II}−N−O_{ox} Torsion Angle

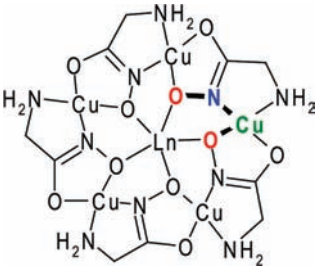

exception is Er3 of **Er-2**). This indicates that the metallacrowns of Type 2B have the same planarity regardless of the central lanthanide ion. The situation is less clear for Type 1; the overall trend is that the oxime oxygen deviation decreases as the metallacrown cavity radius increases. It appears that the metallacrown becomes more planar as the metallacrown cavity decreases. However, the Type 1 metallacrowns are the most difficult to compare. The crystal structures with Nd^{III}, Gd^{III}, and Y^{III} both contain two unique metallacrowns, which are obviously not identical, and each lanthanide is eight-coordinate. While the La^{III} and Pr^{III} structures are even more different, having a nitrate anion bound to the central lanthanide, unlike the others of this type, and the lanthanides are nine-coordinate. The Ce^{III} structure has no bound nitrates to the Ce^{III}, and it is nine-coordinate. This can make it difficult to draw definitive conclusions from the Type 1 data; however, the Type 1 structures are in agreement with the other types of structures. The smaller O_{oxime}−OMP distances for Type 2B indicate that these metallacrowns tend to be the most planar, while the largest O_{oxime}−OMP distances for some of the Type 1 structures implies that these metallacrowns are very ruffled.

Another parameter that reflects the ruffling of the metallacrowns is the O_{oxime}−Cu^{II}−N_{oxime}−O_{oxime} dihedral angle (Scheme 4). If the metallacrown is very planar, then these atoms will lie in the same plane, and the dihedral angle will be very small. If the metallacrown becomes ruffled, then the average dihedral angle will be large as the atoms do not lie in the same plane. A graph showing the average O_{oxime}−Cu^{II}−N_{oxime}−O_{oxime} dihedral angle for each metallacrown plotted against the metallacrown cavity radius is shown in Supporting Information, Figure S45. The general trend in Types 2A, 2B, and 3 is that the dihedral angle decreases as the cavity radius increases. Thus, the metallacrown is becoming more planar as the metallacrown cavity radius increases. Type 1 forms are once again less straightforward because of the variety of structures. At first the dihedral angle decreases (the planarity increases), but then the data reaches a minimum (Nd2 of **Nd-1**) and the dihedral angle increases with an increase in metallacrown cavity radius (the planarity decreases). The largest ruffling is observed for the nine-coordinate **Ce-1** and **La-1** structures.

An additional measure of the planarity of the metallacrown is the distance of each copper(II) ion in the metallacrown ring from the mean plane made by the five copper atoms (the copper mean plane, or CMP). All CMP values were calculated using the SHELXTL software program. A graph showing the average Cu^{II}−CMP distance for each metallacrown is shown in Supporting Information, Figure S46. The general trend seen in Types 1, 2A, and 3 is that the copper(II) ions deviate less from the CMP as

dx.doi.org/10.1021/ic200740h |*Inorg. Chem.* 2011, 50, 7707–7717

Scheme 5. As the $Cu^{II}-Cu^{II}$ Distance Increases the Metallacrown Will Become Less Ruffled

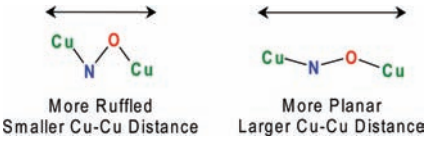

the cavity radius increases. Thus, as the metallacrown cavity radius increases, the metallacrown becomes more planar. For Type 2B, there is virtually no change in the average $Cu^{II}-CMP$ distance as the metallacrown cavity radius increases (the exception is Er3 of **Er-2**). This was also observed for Type 2B $O_{oxime}-OMP$ distances; thus, it seems that these metallacrowns are close to being as planar as possible for all lanthanides and metallacrown cavity sizes. In addition, Type 2B metallacrowns have been shown to be more planar than the other metallacrown types based on the $Cu^{II}-O_{oxime}-N_{oxime}$ and $O_{oxime}-Cu^{II}-N_{oxime}-O_{oxime}$ angle measurements.

Finally, the five $Cu^{II}-Cu^{II}$ distances in each metallacrown were measured to gauge the planarity of the metallacrown. The average $Cu^{II}-Cu^{II}$ distance was plotted against the cavity radius (Figure 8), and the $Cu^{II}-Cu^{II}$ distance increases as the metallacrown cavity radius increases. The trend is clearly observed for all of the types of metallacrowns. Combining this information together with the $Cu^{II}-CMP$ data, it can be seen that the metallacrown changes from being ruffled to more planar as the metallacrown cavity radius increases. The Cu^{II} ions deviate less from the CMP, and they move further apart as the $Cu^{II}-N_{oxime}-O_{oxime}-Cu^{II}$ repeat lies more parallel to the metallacrown plane (Scheme 5). In the same manner, the $O_{oxime}-O_{oxime}$ distance also increases as the metallacrown becomes less ruffled, and so the metallacrown cavity expands.

Thus, as larger lanthanide(III) ions are encapsulated in the metallacrown, the metallacrown cavity expands to accommodate the larger metal ion. As the metallacrown cavity radius increases, the metallacrown becomes less ruffled and more planar as evident by $O_{oxime}-OMP$ distances, $Cu^{II}-CMP$ distances, $Cu^{II}-O_{oxime}-N_{oxime}$ angle measurements, and $O_{oxime}-Cu^{II}-N_{oxime}-O_{oxime}$ angle measurements. The metallacrown becomes less ruffled by increasing the $Cu^{II}-Cu^{II}$ and $O_{oxime}-O_{oxime}$ distances while maintaining constant bond lengths in the molecule. These structural changes are likely the source of the higher observed stability of the 15-MC-5 complexes with the larger Ln^{III} ions.

CONCLUSION

It is evident that within this set of 20 crystal structures, there are both different types of overall metallacrown interactions (mainly dimer formation versus one-dimensional helices) as well as different coordination modes of nitrate anions to the metallacrowns. To draw any conclusions about the effect of an increase of the lanthanide radius on the metallacrown, it is necessary to compare only those structures that have certain criteria in common, in particular the space group and unit cell parameters, as well as lanthanide coordination number and coordination mode of the nitrate anions. Many of the parameters investigated followed the same general trend regardless of the type of metallacrown, while there where cases in which different types of metallacrowns behaved differently.

This series of crystal structures has demonstrated that $Ln^{III}[15\text{-}MC_{Cu^{II}(N)pheHA}\text{-}5]^{3+}$ complexes, where $Ln^{III} = Y^{III}$ and $La^{III}-Tm^{III}$, except Pm^{III}, are hosts for cations that can expand to fit their guest. The metallacrown cavity radius increases linearly with the lanthanide crystal radius expanding to fit the central lanthanide. The lanthanide crystal radii of the smallest (1.07 Å for Tm^{III}) and largest (1.24 Å for La^{III}) lanthanides encapsulated in these structures differ by 0.17 Å. The $Ln^{III}[15\text{-}MC_{Cu^{II}(N)pheHA}\text{-}5]^{3+}$ metallacrowns are able to expand/constrict to accommodate a wide range of metal radii. The distance of the lanthanide to the oxime oxygen mean plane (OMP) is similar for the eight-coordinate lanthanides with lanthanides typically 0.20−0.35 Å from the OMP. However, when the lanthanide becomes "too big" and the cavity cannot expand enough to fit it, the distance increases greatly. The nine-coordinate lanthanides of **La-1**, **Ce-1**, and **Pr-1** are 0.68, 0.65, and 0.62 Å from the OMP, respectively. The data also demonstrates that the OMP and CMP become more planar as the metallacrown cavity increases in size. This is indicated by a decrease in the average $O_{oxime}-OMP$ and $Cu^{II}-CMP$ distances. The $O_{oxime}-Cu^{II}-N_{oxime}-O_{oxime}$ dihedral angles also decrease with an increase in the metallacrown cavity radius. This also indicates that the metallacrown becomes less ruffled as the metallacrown cavity expands. Thus, as larger lanthanides are encapsulated by these $Ln^{III}[15\text{-}MC_{Cu^{II}(N)pheHA}\text{-}5]^{3+}$ complexes the metallacrown cavity radius increases, and the metallacrown becomes more planar by increasing the $Cu^{II}-Cu^{II}$ distance. This detailed investigation into the metrical parameters of the $Ln^{III}[15\text{-}MC_{Cu^{II}(N)pheHA}\text{-}5]^{3+}$ structures may lead to the design of better host−guest metallamacrocyclic complexes.

ASSOCIATED CONTENT

Supporting Information. X-ray crystallographic information of all structures in CIF format. Additional structural descriptions, crystallographic details, numerical parameters, and figures for each compound. This material is available free of charge via the Internet at http://pubs.acs.org.

AUTHOR INFORMATION

Corresponding Author
*E-mail: vlpec@umich.edu.

ACKNOWLEDGMENT

V.L.P. thanks the National Science Foundation for financial support (CHE-0111428).

REFERENCES

(1) (a) Mezei, G.; Zaleski, C. M.; Pecoraro, V. L. *Chem. Rev.* **2007**, *107*, 4933–5003. (b) Pecoraro, V. L.; Stemmler, A. J.; Gibney, B. R.; Bodwin, J. J.; Wang, H.; Kampf, J. W.; Barwinski, A. In *Progress in Inorganic Chemistry*; Karlin, K. D., Ed.; Wiley: New York, 1997; Vol. 45, pp 83−177. (c) Tegoni, M.; Remelli, M. *Coord. Chem. Rev.* **2011**, in press, DOI:10.1016/j.ccr.2011.06.007.

(2) (a) Lah, M. S.; Kirk, M. L.; Hatfield, W.; Pecoraro, V. L. *J. Chem. Soc., Chem. Commun.* **1989**, 1606–1608. (b) Gibney, B. R.; Stemmler, A. J.; Pilotek, S.; Kampf, J. W.; Pecoraro, V. L. *Inorg. Chem.* **1993**, *32*, 6008–6015. (c) Pecoraro, V. L. *Inorg. Chim. Acta* **1989**, *155*, 171–173.

(3) Moon, D.; Lee, K.; John, R. P.; Kim, G. H.; Suh, B. J.; Lah, M. S. *Inorg. Chem.* **2006**, *45*, 7991–7993.

(4) (a) Bodwin, J. J.; Pecoraro, V. L. *Inorg. Chem.* **2000**, *39*, 3434. (b) Pecoraro, V. L.; Bodwin, J. J.; Cutland, A. D. *J. Solid State Chem.* **2000**, *152*, 68–77.

(5) (a) Mezei, G.; Kampf, J. W.; Pan, S. L.; Poeppelmeier, K.; Watkins, B.; Pecoraro, V. L. *Chem. Commun.* **2007**, 1148–1150. (b) Lim, C. S.; Van Noord, A. C.; Kampf, J. W.; Pecoraro, V. L. *Eur. J. Inorg. Chem.* **2007**, 1347–1350.

(6) (a) Stemmler, A. J.; Kampf., J. W.; Kirk, M. L.; Atasi, B. H.; Pecoraro, V. L. *Inorg. Chem.* **1999**, *38*, 2807–2817. (b) Parac-Vogt, T. N.; Pacco, A.; Nockemann, P.; Laurent, S.; Muller, R. N.; Wickleder, M.; Meyer, G.; Vander Elst, L.; Binnemans, K. *Chem.—Eur. J.* **2006**, *12*, 204–210. (c) Parac-Vogt, T. N.; Pacco, A.; Nockemann, P.; Yuan, Y.-F.; Gorller-Walrand, C.; Binnemans, K. *Eur. J. Inorg. Chem.* **2006**, 1466–1474.

(7) Cutland-Van Noord, A. D.; Kampf, J. W.; Pecoraro, V. L. *Angew. Chem., Int. Ed.* **2002**, *41*, 4667–4670.

(8) (a) Cutland, A. D.; Malkani, R. G.; Kampf, J. W.; Pecoraro, V. L. *Angew. Chem., Int. Ed.* **2000**, *39*, 2689–2691. (b) Cutland, A. D.; Halfen, J. A.; Kampf, J. W.; Pecoraro, V. L. *J. Am. Chem. Soc.* **2001**, *123*, 6211–6212. (c) Lim, C. S.; Van Noord, A. C.; Kampf, J. W.; Pecoraro, V. L. *Eur. J. Inorg. Chem.* **2007**, 1347–1350. (d) Mezei, G.; Kampf, J. W.; Pan, S.; Poeppelmeier, K.; Watkins, B.; Pecoraro, V. L. *Chem. Commun.* **2007**, 1148–1150.

(9) (a) Severin, K. *Coord. Chem. Rev.* **2003**, *245*, 3–10. (b) Piotrowski, H.; Polborn, K.; Hilt, G.; Severin, K. *J. Am. Chem. Soc.* **2001**, *123*, 2699–2700. (c) Piotrowski, H.; Hilt, G.; Schulz, A.; Mayer, P.; Polborn, K.; Severin, K. *Chem.—Eur. J.* **2001**, *7*, 3196–3208. (d) Piotrowski, H.; Severin, K. *Proc. Natl. Acad. Sci. U.S.A.* **2002**, *99*, 4997–5000. (e) Lehaire, M.-L.; Scopelliti, R.; Severin, K. *Inorg. Chem.* **2002**, *41*, 5466–5474. (f) Lehaire, M.-L.; Scopelliti, R.; Severin, K. *Chem. Commun.* **2002**, 2766–2767. (g) Lehaire, M.-L.; Scopelliti, R.; Piotrowski, H.; Severin, K. *Angew. Chem., Int. Ed.* **2002**, *41*, 1419–1422. (h) Grote, Z.; Lehaire, M.-L.; Scopelliti, R.; Severin, K. *J. Am. Chem. Soc.* **2003**, *125*, 13638–13639. (i) Grote, Z.; Scopelliti, R.; Severin, K. *Angew. Chem., Int. Ed.* **2003**, *42*, 3821–3825. (j) Lehaire, M.-L.; Schultz, A.; Scopelliti, R.; Severin, K. *Inorg. Chem.* **2003**, *42*, 3576–3581.

(10) (a) Zaleski, C. M.; Depperman, E. C.; Dendrinou-Samara, C.; Alexiou, M.; Kampf, J. W.; Kessissoglou, D. P.; Kirk, M. L.; Pecoraro, V. L. *J. Am. Chem. Soc.* **2005**, *127*, 12862–12872. (b) Zaleski, C. M.; Depperman, E. C.; Kampf, J. W.; Kirk, M. L.; Pecoraro, V. L. *Angew. Chem., Int. Ed.* **2004**, *43*, 3912–3914. (c) Zaleski, C. M.; Kampf, J. W.; Mallah, T.; Kirk, M. L.; Pecoraro, V. L. *Inorg. Chem.* **2007**, *46*, 1954–1956. (d) Dendrinou-Samara, C.; Alexiou, M.; Zaleski, C. M.; Kampf, J. W.; Kirk, M. L.; Kessissoglou, D. P.; Pecoraro, V. L. *Angew. Chem., Int. Ed.* **2003**, *42*, 3763–3766. (e) Zaleski, C. M.; Depperman, E. C.; Kampf, J. W.; Kirk, M. L.; Pecoraro, V. L. *Inorg. Chem.* **2006**, *45*, 10022–10024.

(11) Kessissoglou, D. P.; Kampf, J. W.; Pecoraro, V. L. *Polyhedron* **1994**, *13*, 1379–1391.

(12) Stemmler, A. J.; Kampf, J. W.; Pecoraro., V. L. *Angew. Chem., Int. Ed.* **1996**, *35*, 2841–2843.

(13) (a) Stemmler, A. J.; Barwinski, A.; Baldwin, M. J.; Young, V.; Pecoraro, V. L. *J. Am. Chem. Soc.* **1996**, *118*, 11962–11963. (b) Pacco, A.; Absillis, G.; Binnemans, K.; Parac-Vogt, T. N. *J. Alloys Compd.* **2008**, *451*, 38–41. (c) Dallavalle, F.; Remelli, M.; Sansone, F.; Bacco, D.; Tegoni, M. *Inorg. Chem.* **2010**, *49*, 1761–1772.

(14) Shannon, R. D. *Acta Crystallogr.* **1976**, *A32*, 751–767.

(15) Christensen, J. J.; Eatough, D. J.; Izatt, R. M. *Chem. Rev.* **1974**, *74*, 351–384.

(16) Moras, D.; Metz, B.; Weiss, R. *Acta Crystallogr., Sect B* **1973**, *29*, 383–388.

(17) Mallinson, P. R.; Truter, M. R. *J. Chem. Soc., Perkin Trans.2* **1972**, 1818–1823.

(18) Lah, M. S.; Gibney, B. R.; Tierney, D. L.; Penner-Hahn, J. E.; Pecoraro, V. L. *J. Am. Chem. Soc.* **1993**, *115*, 5857–5858.

(19) Gibney, B. R.; Wang, H.; Kampf, J. W.; Pecoraro, V. L. *Inorg. Chem.* **1996**, *35*, 6184–6193.

(20) Owen, J. D.; Truter, M. R. *J. Chem. Soc., Dalton Trans.* **1979**, *11*, 1831–1835.

(21) Zaleski, C. M.; Cutland-Van Noord, A. D.; Kampf, J. W.; Pecoraro, V. L. *Cryst. Growth Des.* **2007**, *7*, 1098–1105.

(22) (a) Sun, C. S.; Kampf, J. W.; Pecoraro, V. L. *Inorg. Chem.* **2009**, *48*, 5224–5233. (b) Tegoni, M.; Tropiani, M.; Marchio, L. *Dalton Trans.* **2009**, 6705–6708.

(23) Tegoni, M.; Furlotti, M.; Tropiano, M.; Sun, C. S.; Pecoraro, V. L. *Inorg. Chem.* **2010**, *49*, 5190–5201.